

**MICROSTRUCTURAL CHARACTERISTICS OF TZP/Ni CERMETS
PLASTICALLY DEFORMED AT HIGH TEMPERATURE**

A. Morales-Rodríguez ^a, G. Richter ^b, M. Rühle ^b, A. Bravo-León ^a,
A. Domínguez-Rodríguez ^a, M. Jiménez-Melendo ^{a,*}

^a Departamento de Física de la Materia Condensada, Universidad de Sevilla, Spain

^b Max-Planck-Institut für Metallsforschung, Stuttgart, Germany

ABSTRACT

The microstructure of 3 mol% Y₂O₃-stabilized tetragonal ZrO₂/Ni (TZP/Ni) composites has been investigated for nickel concentrations of 20, 30 and 40 vol% before and after creep tests conducted in argon atmosphere at 1250°C under stresses between 9 and 14 MPa. The microstructures have been characterized using scanning, conventional and high-resolution transmission and analytical electron microscopy. Two types of microstructures were found depending on the presence/absence of percolation in the metal phase. The deformation process strongly affects the percolation threshold due to the elongation of metallic grains and subsequently formation of aggregates. TEM and HRTEM studies in as-received and deformed cermets show the lack of dislocation activity and the absence of secondary phases in both zirconia/zirconia and zirconia/nickel interfaces and triple junctions.

Keywords: Cermets; ZrO₂; Creep; Grain boundaries.

1. INTRODUCTION

Ceramic-metal composites (cermets) are interesting materials that combine the properties of metallic inclusions and a ceramic matrix. Among them, the system TZP/Ni is very attractive because nickel and zirconia are relatively inexpensive, chemically stable and immiscible with each other over a wide range of temperatures. They are promising candidates for high added-value functional applications in temperature and flow sensors, thermal protectors for supersonic propulsion systems, and especially as anodes for solid oxide fuel cells (SOFC) [1-4].

The percolation threshold of zirconia/nickel composites, measured by means of electrical conductivity experiments, lies at a nickel concentration of 30-35 vol% [5,6]; conduction is ionic below this value and electronic above it. Complex impedance measurements in wet-processed monolithic TZP/Ni cermets [7] have shown that the percolation threshold appears at a critical content of 34 vol% (more than twice the value predicted by classical percolation theory in disordered systems), where the relative dielectric constant reaches a value close to 1000. This abnormally high percolation threshold in these cermets has been related to the existence of a partial first-neighbour ordering of the metallic inclusions inside the ceramic matrix [7]; this ordered microstructure opens the possibility of new applications of zirconia/nickel composites as electromechanical sensors.

The potential applications of these cermets require the study of their mechanical response, especially at high temperatures, which is strongly affected by the microstructure: particle size, phase distributions, porosity, nature of grain boundaries interfaces, etc. In a preliminary work [8], it was shown that the high-temperature mechanical behaviour of

TZP/Ni composites depends critically on the Ni volumen fraction. The present study is devoted to the microstructural characterization of such cermets with metallic contents below, close to and above the percolation level. The objective is to evaluate the microstructural evolution during high-temperature plastic deformation in order to get a deep understanding of the kind of defects involved in the process.

2. EXPERIMENTAL PROCEDURE

Cermets with relative nickel contents of 20, 30 and 40 vol% (hereafter referred as Ni20, Ni30 and Ni40, respectively), fabricated from high-purity ZrO₂ stabilized with 3 mol% of Y₂O₃ (TZP) and nickel powders and sintered at 1430°C in reducing atmosphere, were supplied by ICMN (Instituto de Ciencia de Materiales-CSIC, Madrid, Spain); details of the processing route can be found in [7,9]. The bulk densities, determined by measuring the dimensions and weight, were about 85% of the respective theoretical values calculated according to the rule of mixtures by taking 6080 and 8900 kg·m⁻³ as the densities of TZP and Ni, respectively.

Plastic deformation tests were carried out in a compressive creep machine in argon atmosphere at 1250°C under stresses of 9-14 MPa. The tests were terminated at a true strain of 45%, without signals of macroscopic failure. A detailed study of the mechanical results and deformation mechanisms in these cermets is given elsewhere [8,10].

The microstructural characterization of the as-received and deformed composites was carried out using scanning and conventional transmission electron microscopy (Microscopy Service-CITIUS, University of Seville, Spain) and by high-resolution

transmission and analytical electron microscopy (Max-Planck Institute for Metal Research, Stuttgart, Germany).

Sections for SEM observations were cut from the samples (parallel to the compression axis in deformed specimens), polished metallographically and thermally etched in reducing atmosphere (90% Ar/10% H₂) at 1250°C for 30 min. The morphological

parameters of both phases: equivalent planar diameter, $d = \left(\frac{4 \cdot \text{area}}{\pi} \right)^{1/2}$; form factor,

$F = \frac{(\text{perimeter})^2}{4\pi \cdot \text{area}}$; and orientation angle of the largest diameter of particles with a fixed

direction (arbitrary in the case of undeformed samples and parallel to the loading axis in deformed specimens), θ , were measured on SEM micrographs by using a semiautomatic image analyzer. The radial distribution function of the nickel particles was determined on these micrographs using a digital treatment described elsewhere [7].

TEM samples were prepared following the conventional techniques of mechanical grinding, dimpling and ion milling of sliced sections, and examined using a Philips CM200 electron microscope operating at 200 kV. HRTEM observations of TZP/TZP grain boundaries and TZP/Ni interfaces were performed in a JEOL JEM-ARM1250 microscope with a point to point resolution of 0.12 nm. Finally, the chemical composition of grain boundaries and interfaces was measured in a dedicated STEM VG HB501 UX for analytical electron microscopy, equipped with a thin window Noran EDS detector; analytical signals were obtained by a spatial difference method [11] from spectra of regions of 3 nm x4 nm containing edge-on interfaces or bulk zones.

3. RESULTS AND DISCUSSION

3.1 Microstructure of as-received materials

The microstructures of as-received Ni20, Ni30 and Ni40 cermets are shown in Fig. 1. The nickel particles (white color) are homogeneously distributed throughout the ceramic matrix (gray) in the three materials. The morphological parameters of the nickel phase are summarized in Table 1. In Ni20 and Ni30, the inclusions are almost spherical ($F = 0.9$) and well isolated from each other; a Gaussian law fits correctly the particle size distributions, giving an average size close to $0.9 \mu\text{m}$ with a standard deviation of about $0.5 \mu\text{m}$. In Ni40, however, some degree of contact between neighbour inclusions is observed, according to its metal content above the percolation limit. The particle contact leads to larger values of both the mean particle size ($1.2 \mu\text{m}$) and the standard deviation ($0.8 \mu\text{m}$), as well as a slightly smaller value for the form factor $F = 0.8$. No preferential orientation of the nickel inclusions was observed in either case.

On the other hand, the zirconia matrix exhibits an equiaxed ($F = 0.9$) and much finer-grained microstructure (Fig. 2). The grain size distributions are consistent with a lognormal law as found in the monoliths [12], with an average apparent diameter of $0.13 \mu\text{m}$ and a standard deviation of $0.06 \mu\text{m}$ in the three cermets. The addition of secondary phases to ceramic materials significantly reduces the grain growth [13–15]; monolithic TZP's processed by the same route than these cermets exhibit twice larger average grain size.

The porosity (black zones in micrographs) is usually associated to nickel/zirconia interfaces, with pore sizes in between those of the metal and ceramic phases. The densities

reached by the present material preparation route, close to 85%, are 10-15% larger than those obtained conventionally from co-sintering of NiO and zirconia powders and subsequent reduction of NiO to metallic Ni [5,13].

Figure 3a shows the radial self-correlation functions of the nickel phase measured in the set of micrographs shown in Fig. 1. A peak at approximately $0.4 \mu\text{m}^{-1}$ was found in the three cermets, corresponding to a distance among nearest-neighbour inclusions of about $2.5 \mu\text{m}$. The independence of the average distance between nickel inclusions with metal concentration agrees with previous observations of Pecharromán et al. [7]; the authors related this feature to a partial first-neighbour ordering of the metallic particles inside the zirconia matrix, probably due to the nature of the wet-processing route chosen to prepare the cermets.

TEM observations showed the absence of dislocations in both ceramic and metal phases. Zirconia grains are stabilized in the tetragonal phase, without the characteristic twinned aspect of the monoclinic symmetry; X-ray diffraction analysis corroborated that the zirconia matrix is almost 100% tetragonal. In the current study HREM observations were used to characterize the structure of the interfaces in the cermets. Fig. 4 depicts high-resolution electron micrographs of zirconia/zirconia and zirconia/nickel edge-on boundaries in Ni20. As can be seen, lattice fringes from differently oriented adjacent particles meet at the boundary, indicating neither secondary phases nor amorphous films are formed along the boundaries. The same results were found in all boundaries examined for the three cermets.

The presence or absence of glassy phases along grain boundaries in TZP ceramics is at present a matter of controversy [14-16]. Very recently, Gremillard et al. [16] have partially rationalized the discrepancies noting that these secondary phases appear only in quenched materials and not in slowly cooled one regardless of the sample purity; by contrast, these phases systematically form glass pockets at multiple grain junctions in impure TZP ceramics. Special attention was therefore paid to these junctions which, as shown in Fig. 5, are also free of any glassy phase. This result is consistent with the high purity of the initial powder and the proper fabrication process [7,9].

Fig. 6 shows energy dispersive spectra (EDS) of two adjacent TZP grains and their common interface. Some segregation of yttrium to the grain boundaries has been observed with an enrichment factor of about 2 with respect to the overall yttria content of the cermets, similar to the level reported for monolithic zirconia regardless of overall yttria content and impurities [17,18]. No evidence of other impurity segregation was found except for iron. The presence of this element at grain boundaries may be due to the reduction of Fe_2O_3 to FeO during the sintering process in reducing atmosphere, that entails Fe segregation from the bulk to the grain boundaries. Recently, Bartolome et al. [20] have shown that the increase of oxygen vacancies concentration by sintering in an inert atmosphere and the presence of Fe^{2+} ions at grain boundaries are responsible for the darkening of 3 mol%-yttria-stabilized tetragonal zirconia.

From this study, it can be concluded that the as-received cermets with a metal concentration below the percolation threshold are formed by individual metallic inclusions surrounded by tetragonal zirconia grains forming a continuous matrix, and by two interpenetrated continuous phases when the metal content is above the threshold

value for percolation. Regardless of the metal/zirconia ratio, zirconia/zirconia and zirconia/nickel interfaces as well as multiple grain junctions are free of glassy phases.

3.2 Microstructure of deformed cermets

Fig. 7 shows the microstructure of Ni20, Ni30 and Ni40 cermets after deformation up to 45% at 1250°C. The zirconia matrix does not undergo significant changes showing the same values than in as-received condition of grain size, form factor and orientation angle. This is consistent with the sluggish grain growth [21] and superior ductility (grain boundary sliding) [13] exhibited by TZP ceramics.

By contrast, the metal phase shows significant changes with respect to undeformed materials. As can be seen in Fig. 7, the particles acquire an elongated shape with the largest diameter oriented preferentially perpendicular to the loading axis; the elongation increases with increasing the nickel content (Table I). There is also an approaching among nickel inclusions in the direction normal to the loading axis, resulting in metal particle contact even in Ni20 and Ni30 which were nominally below the percolation threshold; the contact is more pronounced in samples with larger Ni content. This point was confirmed by electrical resistivity measurements performed on polished sections of the cermets parallel to the compressive axis using a Keithley 2000 multimeter connected to a two-point cell with a distance between points of 2 mm. In contrast with the as-received samples, both Ni20 and Ni30 become conductors after 45% strain with a resistivity of 11.0 and 1.2 Ω -cm, respectively. The increase in particle contact due to deformation is also reflected in the average value and standard deviation of the inclusion size distributions (Table I), specially in Ni30 and Ni40, which show a significant increase with

respect to the as-received conditions. The metal content in Ni20 is too far away from the percolation limit to note this effect in the measurements of the morphological parameters (at least, for strains up to 45%).

In addition, metal defective areas were observed in the samples after deformation, as shown in Fig. 8. These areas are homogeneously distributed in Ni40 with a mean size of about 20 μm . Their densities and size decrease when decreasing the nickel content being hardly observed in Ni20. The redistribution of the nickel phase is due to the particle contact promoted by the deformation. Martínez-Fernández et al. have described similar microstructures consisting in regions free of Si in deformed SiC-Si composites [22].

The radial self-correlation functions of nickel phase in deformed samples are shown in Fig. 3b. The original maximum is slightly displaced from the starting position to values of higher k and a second peak appears in $F(k)$ in the small k values region after deformation. These observations are consistent with the preferential orientation introduced by deformation: inclusions are elongated in the direction perpendicular to the loading axis but shrunk along the parallel one (Fig. 7). Consequently, the original ordering is split into two peaks in the radial distribution representation, each corresponding to parallel and perpendicular directions to the stress axis. As already noted from the SEM micrographs, the deformation process favours the contact between metallic particles forming clusters. In Ni20, the clusters have a relatively uniform size, thus giving a clear division in the radial function because the anisotropy between parallel and perpendicular directions is more outstanding. In the case of Ni40, a previously percolated system, nickel aggregates have a fractal geometry; this microstructure implies an invariant particle size

distribution along the length scale and consequently the self-correlation function $F(k)$ becomes rather constant. Ni30 behaves in between the two extremes.

TEM and HRTEM observations of deformed cermets showed the same features reported above for the as-received materials. In particular, it was found that no amorphous film was formed along the TZP/TZP and TZP/Ni interfaces (Fig. 9) and multiple grain junctions. The same levels of yttrium and iron segregation to grain boundaries than prior to deformation were measured. to grain boundaries than prior to deformation were measured. These microstructural results, along with the mechanical data [10], suggest that the high-temperature plastic deformation of TZP/Ni cermets is controlled by the deformation of the zirconia matrix by means of a grain boundary sliding mechanism.

4. CONCLUSIONS

The microstructure of as-received and high-temperature deformed TZP-Ni cermets with 20, 30 40 vol% nickel contents has been studied. The relative densities of as-received materials are about 85%. Below the percolation threshold (34 vol%), the cermets consist of isolated nickel inclusions homogeneously embedded into a very fined-grained zirconia matrix; above the percolation limit, the material can be described as two interconnected continuous phases.

After uniaxial compression at high temperatures in reducing atmosphere, the ceramic matrix does not undergo any significant change because of its superior ductility. The metal inclusions elongate in the direction perpendicular to the loading axis, resulting in the formation of clusters; the effect is more pronounced for higher nickel contents. Ni20

shows the onset of percolation changing from insulator to conductor despite its nominal metal concentration is below the percolation threshold. Creep processes modify severely such a limit.

No dislocations were detected in nickel and zirconia phases in the as-received and deformed samples. No secondary phases were found by HRTEM observations at either TZP/TZP and TZP/Ni interfaces or triple grain junctions. Yttrium segregates to grain boundaries with an enrichment level of 2.

AKNOWLEDGEMENTS

The authors would like to acknowledge the financial support awarded by the European Commission Research Directorates (General Marie Curie Host Fellowship programme) and the “Ministerio de Educación y Ciencia” (Spain) through the projects MAT2000-1117 and MAT2003-04199-CO2-02. They are also grateful to S. López-Esteban for material processing and to J. Thomas, M. Kelsch and C. Pecharromán for technical assistance.

REFERENCES

- [1] Reschke, S., Bodganow, C., Engineering Ceramics: New Perspectives through Value-Added (Multi-) Functionality. *Key Eng. Materials*, 1999, 175-176, 1-10.
- [2] Sundeen, J. E., Buchanan, R.C., Electrical properties of nickel-zirconia cermet films for temperature- and flow-sensor applications. *Sensor. Actuators A-Phys.*, 1997, 63, 33-40.
- [3] Aruna, S.T., Muthuraman, M., Patil, K.C., Synthesis and properties of Ni-YSZ cermet: anode material for solid oxide fuel cells. *Solid State Ionics* ,1998, 111, 45-51.
- [4] Minh, N.Q., Ceramic Fuel Cells, *J. Am. Ceram. Soc.*, 1993, 76, 563-588.
- [5] Marinsek, M., Zupan K., Macek, J., Preparation of Ni-YSZ composite materials for solid oxide fuel cell anodes by the gel-precipitation method. *J. Power Sources* 2000, 86, 383-389.
- [6] Koide, H., Someya, Y., Yoshida, T., Maruyama, T., Properties of Ni/YSZ cermet for SOFC. *Solid St. Ionics* 2000,132, 253-260.
- [7] Pecharromás, C., López-Esteban, S., Bartolomé, J.F., Moya, J.S., Evidence of Nearest-Neighbor Ordering in Wet-Processed Zirconia-Nickel Composites. *J. Am. Ceram. Soc.*, 2001, 84, 2439-41.
- [8] Morales-Rodríguez, A., Bravo-León, A., Domínguez-Rodríguez, A., López-Esteban, S., Moya, J.S., Jiménez-Melendo, M., High-temperature mechanical properties of zirconia/nickel composites. *J. Eur. Ceram. Soc.* 23(2003)2849-2856.
- [9] López-Esteban, S., Procesamiento, caracterización eléctrica y mecánica de materiales compuestos 3Y-TZP/Ni. PhD Thesis, Universidad Politécnica de Madrid, Madrid, 2001.
- [10] Morales-Rodríguez, A., Bravo-León, A., Domínguez-Rodríguez, A., Jiménez-Melendo, M., Creep Mechanisms of TZP/Ni cermets. Submitted to *J. Am. Ceram. Soc.*

- [11] Dehm, G., Ernst, F., Mayer, J., Möbus, G., Müllejans, H., Phillipp, F., Scheu, C., Rühle, M., Transmission Electron Microscopy at the Max-Planck-Institut für Metallforschung. In Zeitschrift für Metallkunde 87, ed. C. H. Verlag. München, Germany, 1996, pp. 898-910.
- [12] Bravo-León, A., Jiménez-Melendo, M., Domínguez-Rodríguez, A., Mechanical and microstructural aspects of the high temperature plastic deformation of yttria-stabilized zirconia polycrystals. *Acta metall.*, 1992, 40, 2717-2726.
- [13] Jimenez-Melendo, M., Domínguez-Rodríguez, A. and Bravo-León, A., 'Superplastic flow of fine-grained yttria-stabilized zirconia polycrystals: constitutive equation and deformation mechanisms. *J. Am. Ceram. Soc.*, 1998, 81, 2761–2776.
- [14] French, F. D., Harmer, M. P., Chan, H. M. and Miller, G. A., Coarsening-resistant dual-phase interpenetrating microstructures. *J. Am. Ceram. Soc.*, 1990, 73, 2508–2510.
- [15] Lange, F. and Hirlinger, M., Grain growth in two-phase ceramics: Al₂O₃ inclusions in ZrO₂. *J. Am. Ceram. Soc.*, 1987, 70, 827–830.
- [16] Stathis, G., Simwonis, D., Tietz, F., Moropoulou, A., Naoumides, A., Oxidation and resulting mechanical properties of Ni/8Y₂O₃-stabilized zirconia anode substrate for solid-oxide fuel cells. *J. Mater. Res.*, 2002, 17, 951-958.
- [17] Hines, J. A., Ikuhara, Y., Chokshi, A. H., Sakuma, T., The influence of trace impurities on the mechanical characteristics of a superplastic 2 mol% yttria stabilized zirconia. *Acta mater.*, 1998, 46, 5557-5568.
- [18] Stemmer, S., Vleugels, J., Van Der Biest, O., Grain Boundary Segregation in High-purity Yttria-stabilized Tetragonal Zirconia Polycrystals (Y-TZP). *J. Eur. Ceram. Soc.*, 1998, 18, 1565-1570.

- [19] Gremillard, L., Epicier, T., Chevalier, J. and Fantozzi, G., Effect of cooling rate on the location and chemistry of glassy phases in silica-doped 3Y-TZP ceramics. *J. Eur. Ceram. Soc.* 2005, 25, 875-882.
- [20] Bartolomé, J. F., Montero, I., Diaz, M., López-Esteban, S. and Moya, J. S., 'Accelerated aging in 3-mol%-yttria-stabilized tetragonal zirconia ceramics sintered in reducing conditions. *J. Am. Ceram. Soc.*, 2004, 87, 2282–2285.
- [21] Nieh, T.-G., Wadsworth, J., Dynamic Grain Growth During Superplastic Deformation of Yttria-Stabilized Zirconia Polycrystals. *J. Am. Ceram. Soc.*, 1989, 72, 1469-1472.
- [22] Martínez-Fernández, J., Muñoz, A., Arellano-López, A. R. de, Varela-Feria, F. M., Domínguez-Rodríguez, A., Singh, M., Microstructure-mechanical properties correlation in siliconized silicon carbide ceramics. *Acta mater.*, 2003, 51, 3259-3275.

TABLE CAPTIONS

Table I. Average values and standard deviations of grain size d , shape factor F and orientation angle of the maximum diameter θ , of nickel inclusions in as-received (R) and 45%-strained (S) cermets.

Specimen	\bar{d} (μm)	σ_d (μm)	\bar{F}	σ_F	$\bar{\theta}$ ($^\circ$)	σ_θ ($^\circ$)
Ni20 (R)	0.82 ± 0.03	0.44 ± 0.02	0.88 ± 0.01	0.18 ± 0.01	103 ± 3	40 ± 2
Ni20 (S)	0.85 ± 0.03	0.45 ± 0.02	0.76 ± 0.01	0.22 ± 0.01	91 ± 2	26 ± 1
Ni30 (R)	0.87 ± 0.02	0.49 ± 0.01	0.85 ± 0.04	0.21 ± 0.01	96 ± 3	43 ± 2
Ni30 (S)	1.12 ± 0.05	0.77 ± 0.04	0.70 ± 0.02	0.24 ± 0.01	90 ± 2	27 ± 1
Ni40 (R)	1.18 ± 0.05	0.80 ± 0.04	0.76 ± 0.02	0.24 ± 0.01	89 ± 2	41 ± 2
Ni40 (S)	1.34 ± 0.08	1.07 ± 0.06	0.64 ± 0.02	0.26 ± 0.01	94 ± 2	23 ± 1

FIGURE CAPTIONS

Fig. 1. SEM micrographs of as-received composites: (a) Ni20, (b) Ni30 and (c) Ni40.

Fig. 2. Detail of as-received Ni20 cermet, showing the fine and equiaxed microstructure of the TZP matrix.

Fig. 3. Radial self-correlation functions of metallic phase in: (a) as-received composites; (b) deformed composites ($\sigma = 9 - 14$ MPa; $T = 1250$ °C; $\epsilon_f = 45\%$).

Fig. 4. High-resolution electron micrographs of: (a) TZP/TZP grain boundary; (b) TZP/Ni interface in as-received Ni20 cermet. The reticular planes observed are indicated. No amorphous phase is formed along the boundaries in both cases.

Fig. 5. HRTEM micrograph of as-received Ni20 showing the absence of glassy pockets at a triple junction.

Fig. 6. EDS spectra of two adjacent TZP grains and their common interface. Peaks used in the analysis are indicated by discontinuous lines in *TZP grain 1*. Cu line is due to the copper ring of the TEM sample.

Fig. 7. SEM micrographs of 45%-strained composites (9.5-14 MPa, 1250°C): (a) Ni20, (b) Ni30 and (c) Ni40. The compressive axis is vertical.

Fig. 8. SEM micrographs of deformed Ni40 showing the lost of homogeneity in nickel distribution: (a) low magnification micrograph; (b) detail of a high-porous Ni defective area. The compressive axis is vertical.

Fig. 9. HRTEM micrographs of: (a) TZP/TZP grain boundary; and (b) TZP/Ni interface in strained Ni20. No secondary phases are formed along the boundaries.

Figure 1

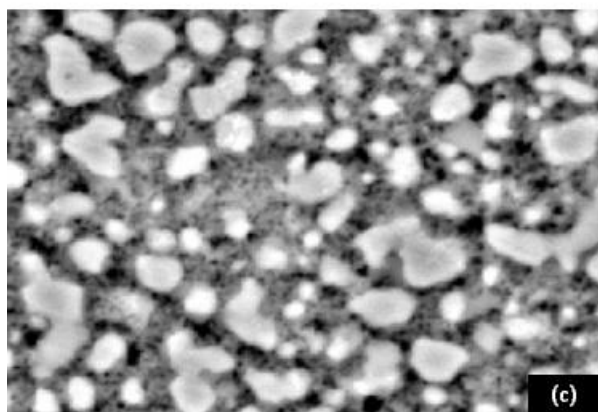
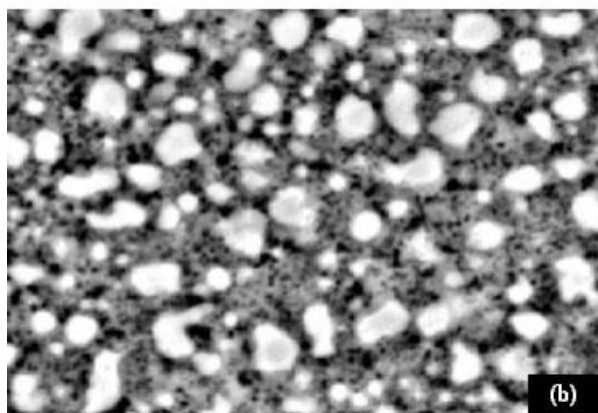
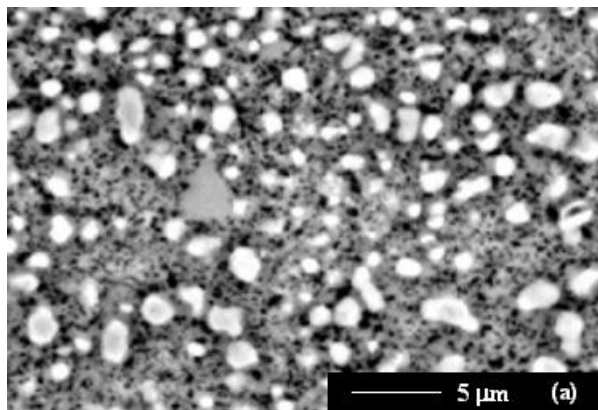


Figure 2

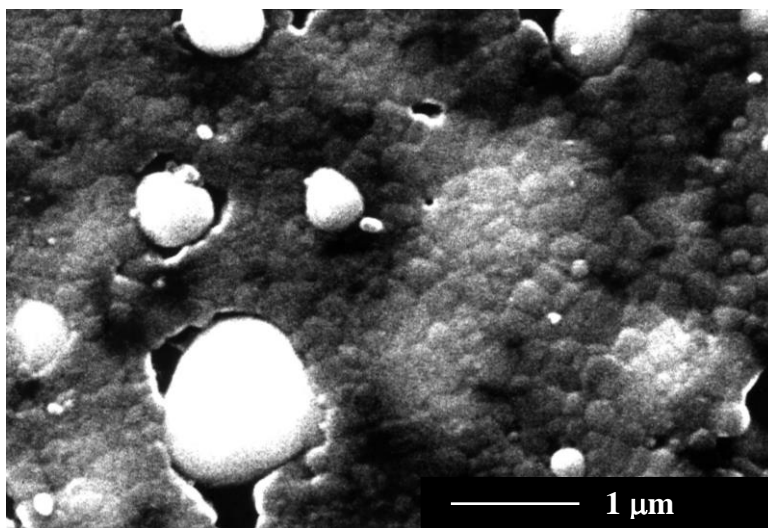


Figure 3

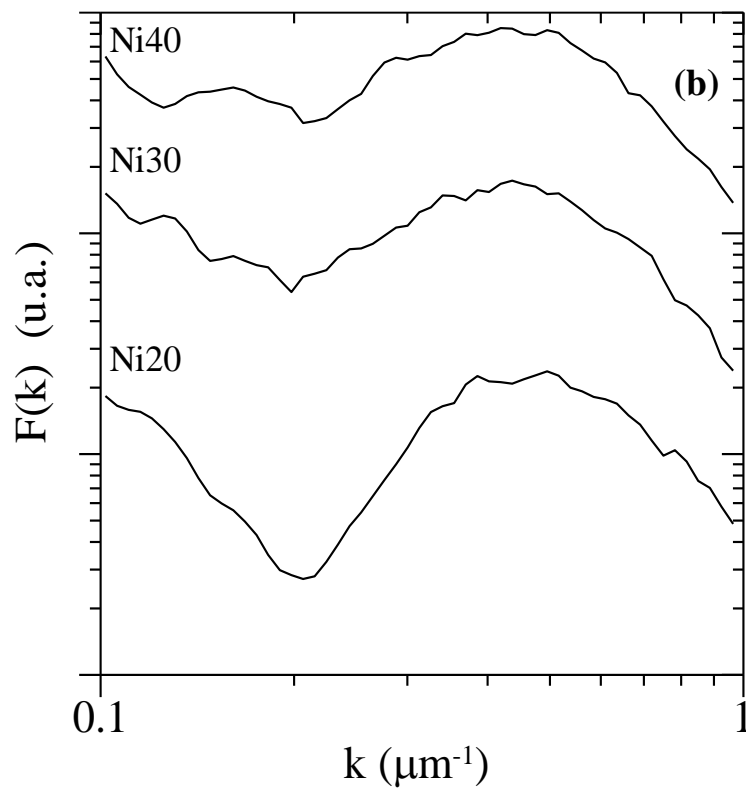
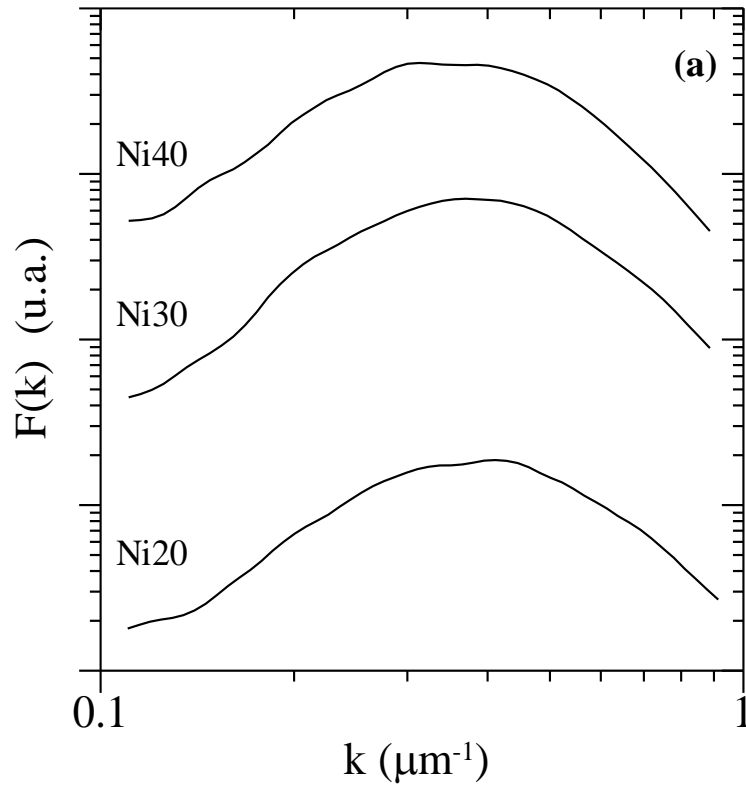


Figure 4

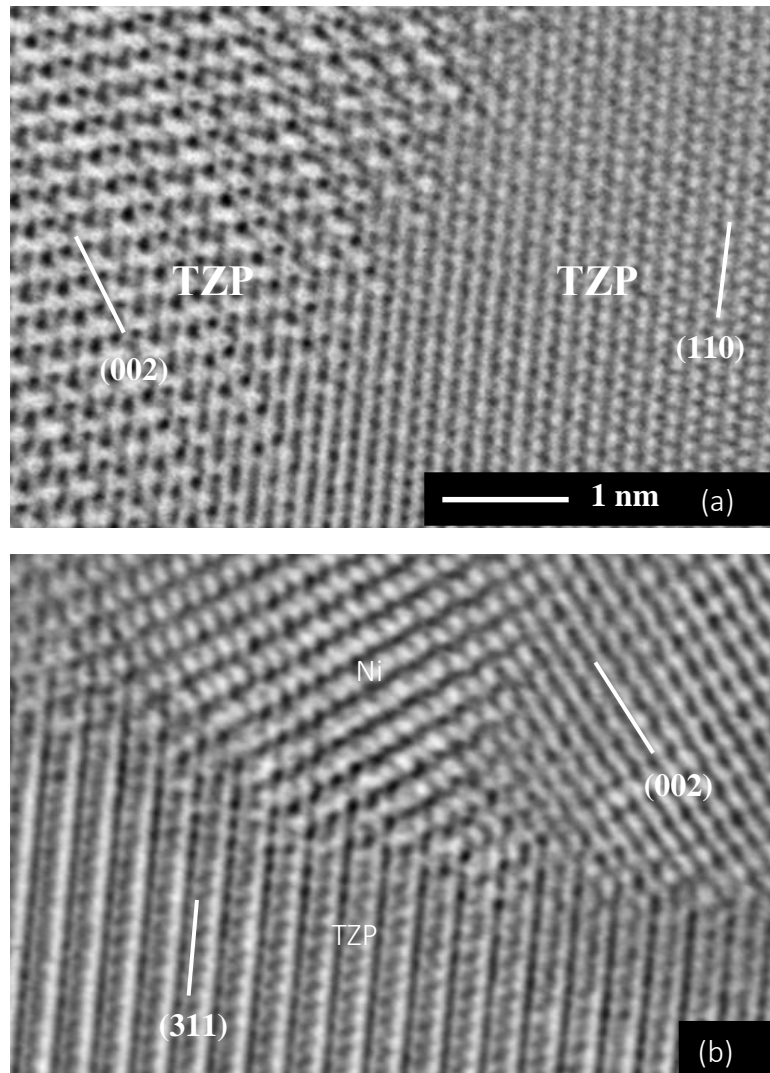


Figure 5

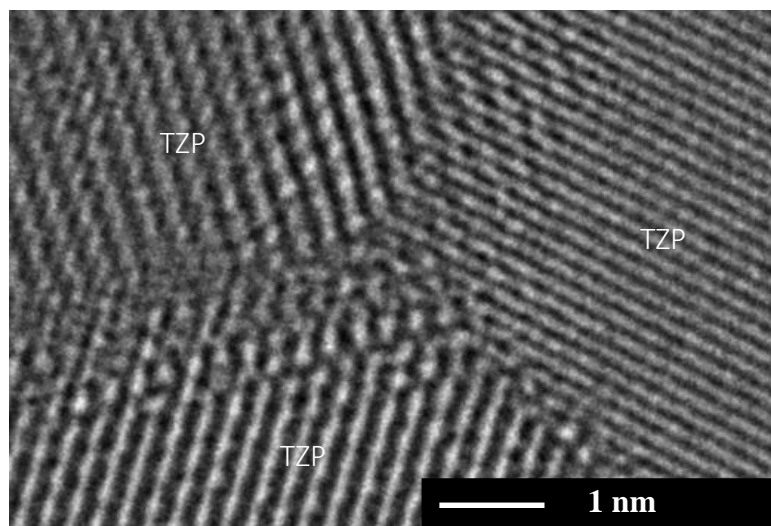


Figure 6

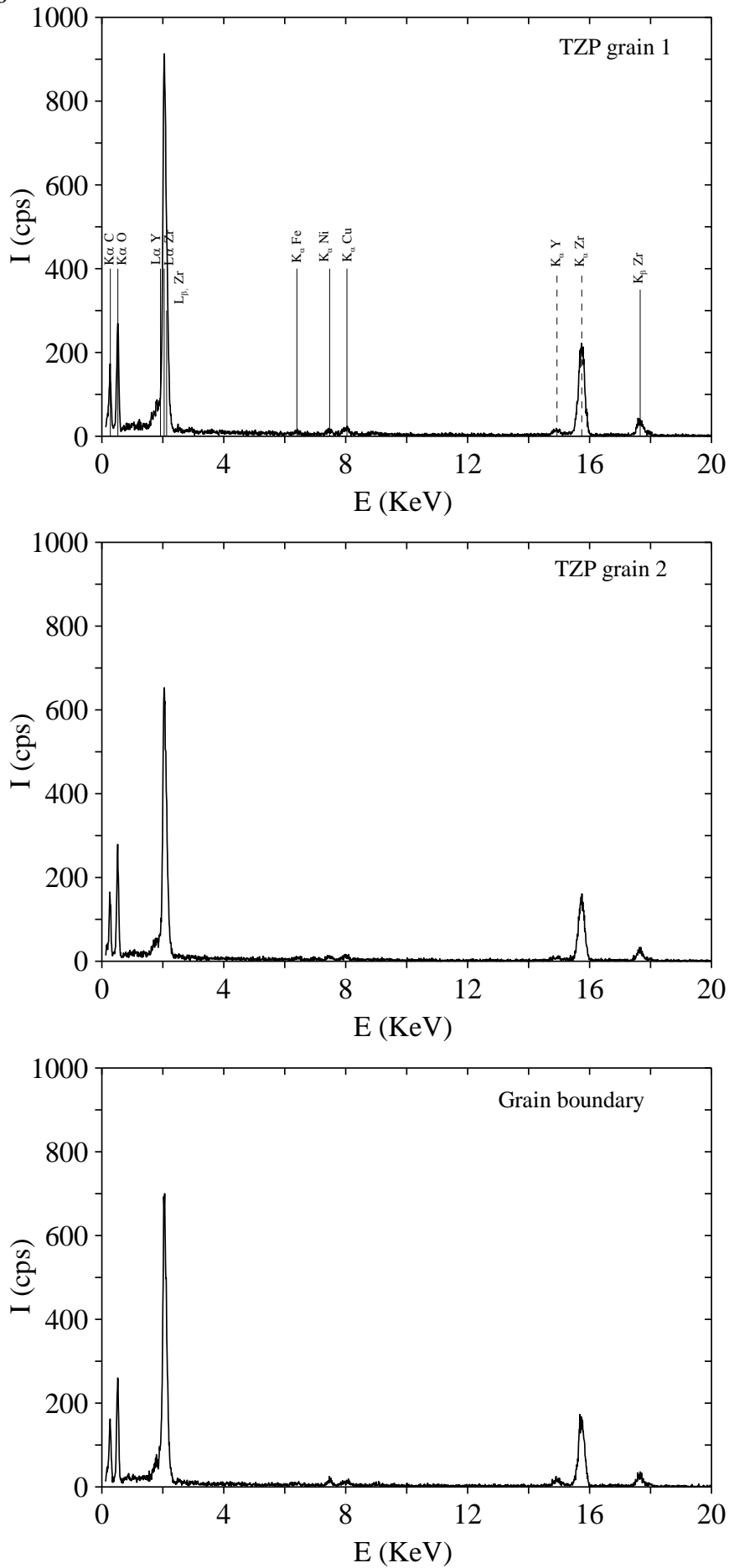


Figure 7

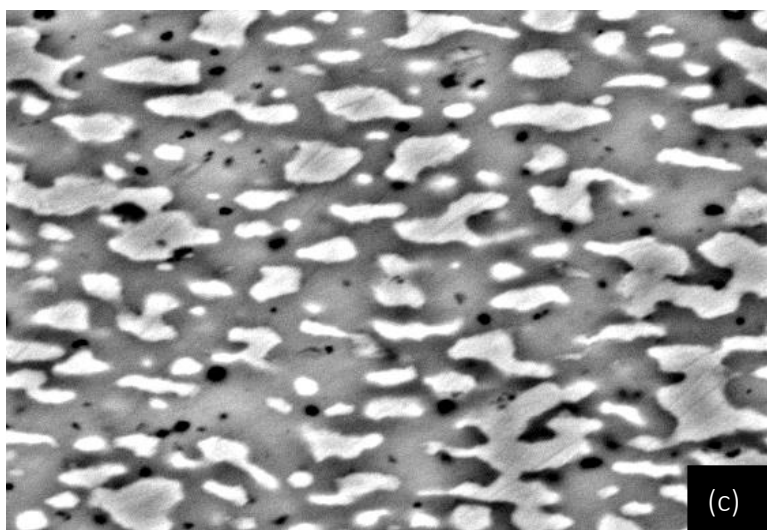
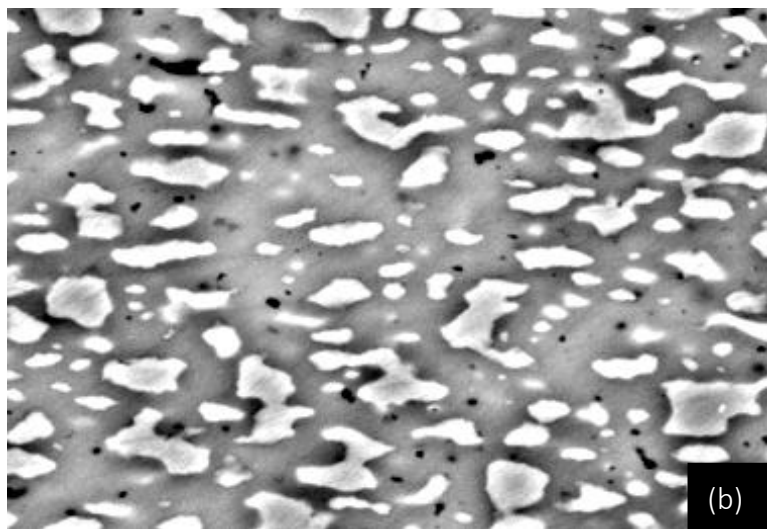
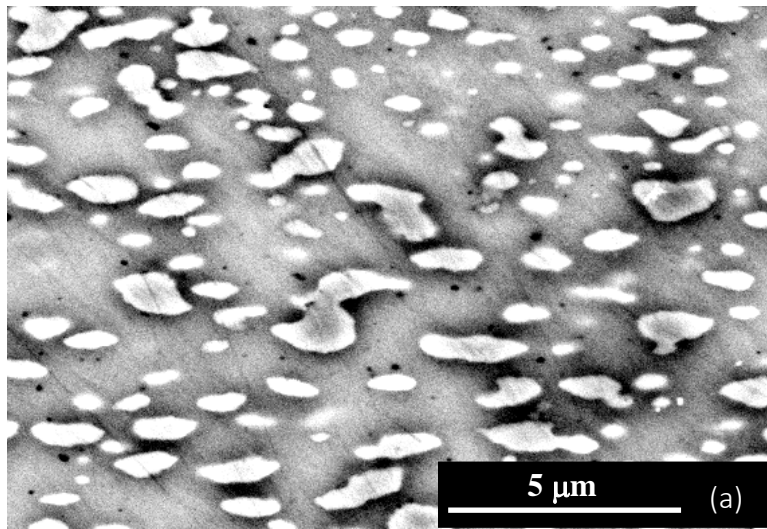


Figure 8

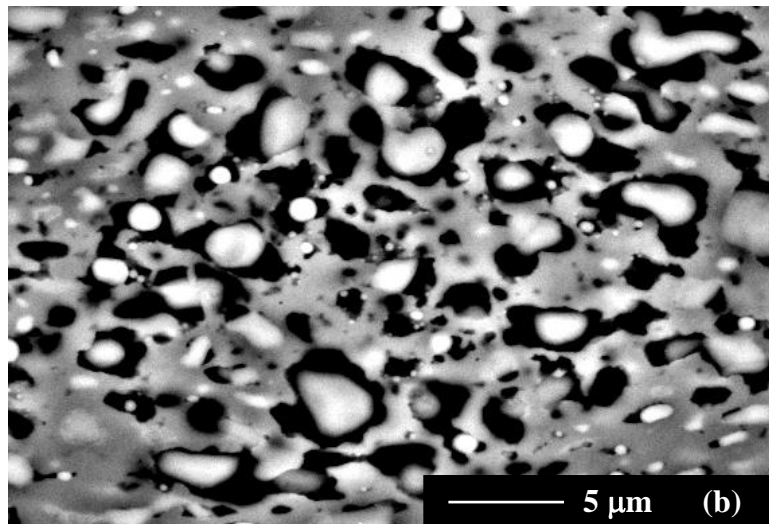
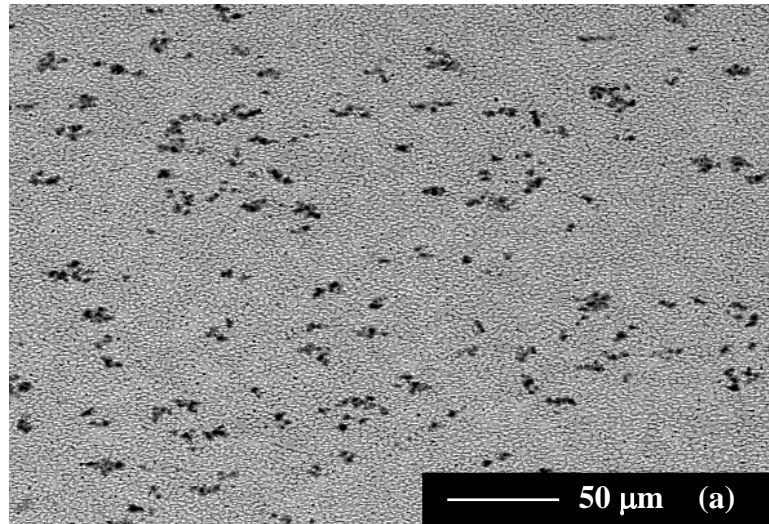


Figure 9

